

150 New transiting planet candidates from *Kepler* Q1–Q6 data

X.Huang^{1*}, G.Bakos¹, J.D.Hartman¹,

¹ Department of Astrophysical Sciences, 4 Ivy Lane, Peyton Hall, Princeton University, Princeton, NJ 08544

5 March 2013

ABSTRACT

We have performed an extensive search for planet candidates in the publicly available *Kepler* Long Cadence data from quarters Q1 through Q6. The search method consists of initial de-trending of the data, applying the trend filtering algorithm, searching for transit signals with the Box Least Squares fitting method in three frequency domains, visual inspection of the potential transit candidates, and in-depth analysis of the shortlisted candidates. In this paper we present 150 new periodic planet candidates and 7 single transit events, 72 of which are in multiple systems. The periods of these planet candidates vary from ~ 0.17 day to ~ 440 day. 124 of the planet candidates have radii smaller than $3 R_{\oplus}$. We recover 82.5% of the Batalha et al. (2012) KOI catalog. We also report 40 newly identified false positives—systems that look like transiting planets, but are probably due to blended eclipsing binaries. Our search improves the statistics in the short period and small planet radii parameter ranges.

Key words: planetary systems-stars: individual

1 INTRODUCTION

The field of transiting extrasolar planets (TEPs) has exploded over the past few years. One major contributor is the *Kepler Space Mission*, continuously monitoring 156000 stars in a $115 \deg^2$ field (Borucki et al. 2010; Koch et al. 2010). Since its launch in 2009, it has found 2321 planetary transit candidates¹ (Borucki et al. 2011a; Batalha et al. 2012). The first 4 months of data (Q1 and Q2) yielded 1235 planet candidates associated with 997 host stars, including 60 confirmed planets around 33 stars (Borucki et al. 2011b, hereafter B11). The *Kepler* team has developed increasingly sophisticated procedures to identify planet candidates (Smith et al. 2012) and multiple systems (Steffen et al. 2012; Ford et al. 2012). Using more data (16 months) and improved detection procedures (the Transit Planet Search (TPS) algorithm; Jenkins et al. 2010c; Tenenbaum et al. 2012), the total number of planet candidates has almost doubled since the release by B11 (Batalha et al. 2012, hereafter B12).

An independent search with different tools can build confidence in the reliability of the detections, and the completeness of the sample, by e.g. providing new candidates that were missed by the *Kepler* science team. One such effort is the citizen science initiative, called PlanetHunters (Fischer et al. 2012; Lintott et al. 2012), based on the idea of Zooniverse (Lintott et al. 2008). Making use of human

eyes to search for transit-like events through a user friendly computer interface, 6 new planet candidates were published by far (Fischer et al. 2012; Lintott et al. 2012). These were then subjected to the vetting procedure of the *Kepler* team, and five of them survived this process, i.e. they are not false alarms, as much as it can be determined from the *Kepler* data. However, conducting a visual search of all the raw light curves takes a lot of human effort. Quoted from Fischer et al. (2012): “It is impractical for a single individual to review each of the $\sim 150,000$ light curves in every quarterly release of the *Kepler* data base.” While challenging, it is, however, feasible for an individual to examine $\sim 150,000$ light curves, if sophisticated computer algorithms narrow down the list to a somewhat smaller sample of candidate transits that can be then checked very carefully. Also, note that small planets are often hard to recover by visual inspection without phase-folding the light curve at the suspected periodicity of the signal.

Encouraged by these observations, we started an independent search for transiting planet candidates in *Kepler*’s long-cadence data. *Kepler* observations are grouped into so-called quarters (each having a duration of 3 months, except for Q0 and Q1, which are shorter). At the end of each quarter, the spacecraft rotates 90 degrees, to adjust its solar panels. The majority of *Kepler* stars are observed as long cadence (LC) targets, for which data are obtained by gathering over 270 exposures within 29.4 min; 512 stars are also observed in short cadence (SC) mode with 58.9 s intervals (Jenkins et al. 2010b; Gilliland et al. 2010; Murphy 2012).

* E-mail:xuhuang@princeton.edu;

¹ <http://kepler.nasa.gov/Mission/discoveries/candidates/>

We used quarters Q0-Q6 in this search, which data were released to the public in Jan 2012.

Our methodology is based on our experience conducting a similar search with HATNet (Bakos et al. 2004), a wide-field ground-based survey. Broadly speaking, the *Kepler* space-based data is of much higher quality than any ground-based data. Ground based observations often exhibit large gaps in the time-series, either due to the rotation of the Earth, or inclement weather conditions. The data quality is highly variable due to changing extinction, clouds, background, seeing, etc. The per-point photometric precision is typically worse than from space, partly because of the above effects of ground-based observations, and partly due to the use of inexpensive hardware (e.g. front illuminated CCDs). Altogether, our ground-based data is of lower signal-to-noise, has inhomogeneous quality, and exhibits complex systematic variations with long gaps. For example, not a single transit event has been found in HATNet data by direct visual inspection; transits are detected through sophisticated data mining and phase-folding. Also, no robust *single* transit event was ever found by HATNet. Consequently, tools developed for a transit search using ground based data may be very efficient in recovering transit signals from *Kepler*.

In this paper we employ tools from the transit detection pipeline of the HATNet project, after sufficient modifications to conform to the *Kepler* data. We also develop a pre-filtering method that corrects the *Kepler* light curves for known anomalies and systematics, before searching them for transit events. Our search is blind in the sense that the list of *Kepler* candidates was not consulted during the search.

The structure of the paper is constructed as follows. The data processing methodology is discussed in §2. We laid out our findings in §3, including the recovery of Kepler planet catalog, our selection and modeling of new candidates, and the properties of these new candidates. We make our concluding remarks in §4.

2 DATA ANALYSIS

2.1 Removal of points and long trend filtering

We make use of the *Kepler* public LC light curves. We begin with the TIME and SAP_FLUX (raw flux) columns in the FITS files. The raw flux is already corrected for cosmic rays and background variations by the *Kepler* team (Jenkins et al. 2010a). First we convert the fluxes to magnitudes and set the mean value for each star to its *Kepler* magnitude taken from the Kepler Input Catalog (KIC)².

The second step is to clean the light curves based on the data anomalies table in the *Kepler Data Release Notes* for each quarter (Christiansen et al. 2012,b; Machalek et al. 2010, 2011). We summarize all the important events in Q1 through Q6 in Table 1. We also describe the definition of anomaly types (adopted from *Kepler Data Characteristic Hand Book*) and our methods of correction for each type in the table notations. Generally, for data anomalies involving a discontinuity we model the jump by a polynomial with an offset in magnitude after the gap. The fitting uses 50 points

on both sides around the gap. The offset is then subtracted from the data after the jump. In the time range during safe modes (Q2 and Q4), or earth point recoveries (Q3, Q4 and Q6), there is an exponential decay in the flux. We identify and remove the whole exponential decay rather than attempting to correct for the effect.

Most of the stars exhibit long-term trends. We follow the traditional high-pass filter method (Ahmed et al. 1974; Mazeh & Faigler 2010), and apply a cosine filter on all the cleaned light curves. For each light curve, before computing the filter, we generate a model by applying a 100 point (~ 2 day long) median filter. This is done to prevent distortions due to outlier points (including introducing spurious “transit” signals). The cosine filter is then computed as the sum of a linear component and $N = T_{total}/\Delta T$ cosine functions, where the highest frequency is $1/\Delta T$ ($\Delta T = 1$ day), and T_{total} is the total time span of the light curve:

$$M(t_j) = a \frac{(t_j - t_s)}{T_{total}} + \sum_{i=0,N} b_i \cos \left[i\pi \frac{(t_j - t_s)}{T_{total}} \right]. \quad (1)$$

Here t_j is the time of the j th measurement, and t_s is the first time instance in the light curve. The coefficient a for the linear component and coefficient b_i for the i th cosine functions are computed by a least squares fitting procedure on the model. The fitted trend $M(t_j)$ is then subtracted from the light curves. We apply this cosine filter to light curves in every Quarter separately, and then combine the long trend filtered light curves from Q1-Q6 by offsetting the magnitude of all the quarters referring to the magnitude of Q1.

2.2 Sky groups and Systematic Trend filtering

Following the long-term trend filtering procedure described above (§ 2.1), we then apply the Trend Filtering Algorithm (TFA) developed by Kovács et al. (2005) on the combined (Q1–Q6) light curves. The idea of TFA is to select a set of template light curves, which we assume to contain information of the systematic variations, and then construct a linear filter based on their shared time-series for each light curve to be corrected. TFA can remove systematic variations that are either shorter time-scale than those corrected by the cosine filter, or have an arbitrary functional form that is not well described by the sum of cosine functions. TFA assumes that the light curves are sampled at the same time-instances.

To construct a set of template light curves with the same time-base, we make use of the sky group information provided by the *Kepler* team. The sky group number is defined as the CCD channel number on which the stars fell during Q2 of the *Kepler* operation. *Kepler* has 21 modules. Each module contains 2 CCD chips and each CCD contains 2 output channels. The focal plain rotates 90 degrees when the telescope switches to a new quarter every 3 months, except for the initial transition between quarters Q0 to Q1. Generally, the stars that belong to the same sky group share the same CCD channel all the time, although this channel changes from time to time. Therefore, each sky group shares the same time base, and has similar instrumental systematic trends. Additionally, stars in the same sky group are related in terms of their sky position, so that the local variabilities (e.g. local background variations or flux contamination from nearby stars) are often shared. TFA is designed to reduce

² <http://tdc-www.harvard.edu/software/catalogs/kic.html>

this kind of general (shared by a number of stars) systematics.

We construct a separate filter for each sky group, selecting ~ 300 template light curves in each case. Template stars are selected randomly, but in a manner that ensures a uniform distribution of their positions across the field. To exclude variable stars, we also impose a constraint on their median deviation around the median magnitudes (MAD, a quantity that is insensitive to outliers); stars with high MAD are ruled out from the templates. The total number of data points (time samples) in each template time base is $\sim 17000 - 22000$, depending on the total length of time series in the sky group. In other words, we are not overfitting the light curves.

Altogether 124840 stars in 84 sky groups were selected and analyzed with TFA from the *Kepler* public LC data. For each sky group, we only selected stars that have been observed during the complete time range, and have not been affected by the failure of module 3. This is because the TFA analysis requires the same time-base to generate the filter per sky group. Module 3 failed in the middle of Q4, while observing sky groups 5, 6, 7 and 8. Due to the rotation of spacecraft, the Q5 data in sky groups 49, 50, 51 and 52, and the Q6 data in sky groups 77, 78, 79, and 80 were not available. Stars in these sky groups are still included if they have a complete data set in other quarters. Otherwise, we only selected light curves containing all the Q1-Q6 data (which has a total observation time of ~ 500 days).

We note that the *Kepler* team has recently implemented a new “cotrending” algorithm, called PDC-MAP (Smith et al. 2012). This algorithm uses 16 Cotrending Basis Vectors (CBV) that are generated by a singular value decomposition method applied separately to each channel and each quarter. This method has some commonalities with TFA. We did not make use of the PDC-MAP data, since it was not available for the Q1–Q6 data when we started our analysis.

In Figure 1 we demonstrate our filtering process on a randomly selected light curve (KIC003346154). The great improvement by the procedure is clearly demonstrated.

2.3 Box Least Square Fitting (BLS) and Transit Analysis

We use the box least square fitting algorithm (Kovács et al. 2002) to search for periodic transit signals in the TFA-filtered light curves. In order to maximize the efficiency of the BLS search in a wide frequency range, we divide the frequency search into three, only slightly overlapping frequency domains: $0.3 \text{ d}^{-1} < f_1 < 9.0 \text{ d}^{-1}$, $0.02 \text{ d}^{-1} < f_2 < 1.0 \text{ d}^{-1}$ and $0.005 \text{ d}^{-1} < f_3 < 0.03 \text{ d}^{-1}$. We use a different number of frequency steps and BLS bins in each domain. We use the SNR (signal to noise ratio, measured in the BLS spectrum) and DSP (dip significance) parameters (for details, see Kovács et al. 2002) of the first five frequency peaks reported by BLS to select candidate transit signals for manual inspection.

We adopt selection threshold of 11 and 8.5 for SNR and DSP in the middle and long period range. The selection threshold of short period range is somewhat higher (30 and 20 for SNR and DSP) considering that BLS tends to respond to short period easier and there are fewer KOIs in this period range as our reference. On top of these requirements,

we neglect the BLS peaks with frequency too close to the frequency domain boundary (i.e. the period ranges used in selection are $0.67 \text{ d}^{-1} < f'_1 < 6.67 \text{ d}^{-1}$, $0.0202 \text{ d}^{-1} < f'_2 < 0.67 \text{ d}^{-1}$ and $0.005 \text{ d}^{-1} < f'_3 < 0.0202 \text{ d}^{-1}$). We also reject those with a transit duration much longer than expected ($q_1 < 0.5$, $q_2 < 0.1$ and $q_3 < 0.013$) or a transit depth indicating very large planetary radius ($dip > 0.04$). These are not optimized selection criteria, but instead ensure that no shallow or rare transit events are missed. The low detection threshold also means that events will require close visual inspection. With the above limits, we selected $\sim 10\%$ of the stars to fold with the BLS peaks that satisfy the above requirements. The number of BLS peaks selected is $\sim 3\%$ of all the first five best BLS peaks. We then manually inspected all the folded light curves.

We take three random sky groups as an example to illustrate our selection process in Figure 2. We show the distribution of BLS peaks (the mid period range) in the SNR-DSP plane. The solid lines are our lower limits for selection. The green dots are selected periods for further examination. The best BLS peak of KOI planet candidates are represented with red crosses. Majority of the KOIs are selected with high SNR and DSP.

Transit-like features in the folded light curves are flagged and further examined in the visual inspection. We reject light curves with recognizable depth variation for odd and even peaks. We also check the harmonics of the detected period to ensure the detection of a correct period. For the transits visible in the unfolded light curves, we directly inspect the shape and transit center of each transit; for the transits invisible in the unfolded light curves (due to low S/N), we perform phase-folding with the BLS-detected frequency before examining the data.

3 RESULTS

3.1 Comparison of Our Sample to that of the *Kepler* Team

We flagged 2180 stars as possible transiting planet hosts during manual inspection. Among them, we found 180 stars which are categorized as eclipsing binaries (EB)³ (Prša et al. 2011) or false positives (FP)⁴ (Borucki et al. 2011b) by the *Kepler* team. We also cross-matched our results with the KOI catalog⁵ (Borucki et al. 2011a,b; Batalha et al. 2012). We note that our detection efficiency is comparable to the TPS algorithm used by the Kepler team (Tenenbaum et al. 2012, Hereafter T12). Their algorithm yields 5392 detections and detected 88.1% of the 1235 KOIs in the B11 catalog using data from Q1–Q3. We recovered 92% of the B11 catalog in our analysis (1124 of the KOIs in B11 are in our initial data set, from which, 1034 are flagged) thanks to the longer time base we used compared to T12.

We demonstrate the selection of KOIs compared to the B12 catalog in Figure 3. There are 1518 KOI stars (corresponding to 1982 KOI planet candidates) from the B12 catalog included in our overall LC light curve samples. The rest

³ http://archive.stsci.edu/kepler/eclipsing_binaries.html

⁴ http://archive.stsci.edu/kepler/false_positives.html

⁵ http://archive.stsci.edu/kepler/planet_candidates.html

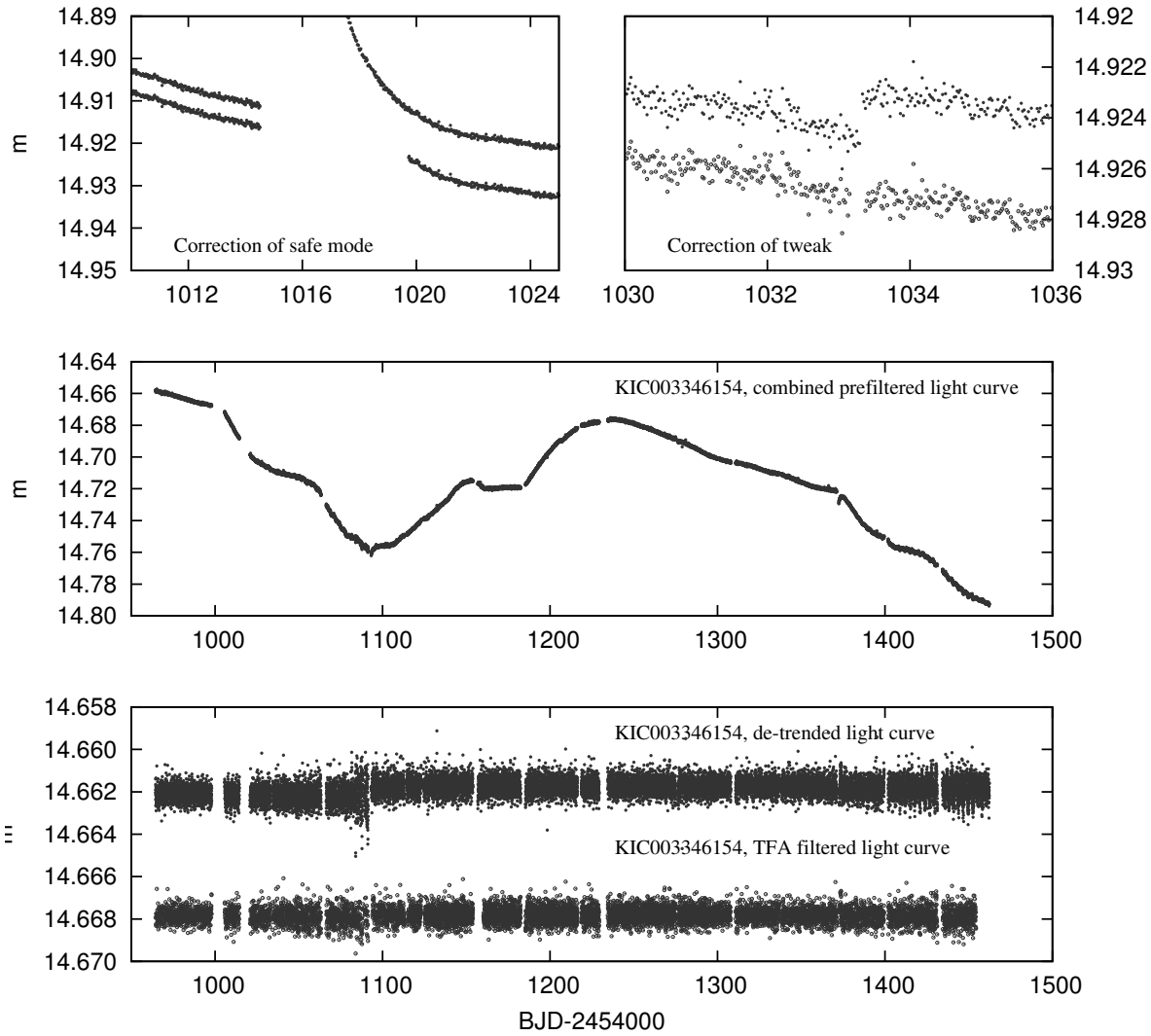


Figure 1. An example of our filtering process as applied to the light curve of KIC 003346154. The ordinate is in the units of approximate *Kepler* magnitude: Top panel: correction of safe mode (left) and tweak (right), (the example is taken from Q2). The corrected light curve is plotted below the uncorrected one. Middle panel: combined light curve from Q1-Q6 after the pre-filtering process, i.e. correction of anomalous data points and combining the light curves from all the quarters. Bottom panel: light curve after long trend filtering (solid symbols) and after TFA (empty circles).

of the KOI stars in the B12 catalog either fail to fulfill our long cadence time baseline length requirement (see §2.2) or have transit depths greater than 0.04, and are therefore rejected by our procedure. We found that 1311 (86.4%) of the KOI stars are flagged in our selection process. 1636 (82.5%) of the KOI planet candidates are detected (either with the correct period reported by BLS or are detected with the wrong period but later recovered during visual inspection).

We failed to recover about 17.5% of the KOI planet candidates, mostly due to no significant peaks found in the BLS spectra corresponding to the transit periods. This partly results from the choice of BLS parameters and also the non-

periodic properties of some transit signals. The hard cut in DSP is the second most important reason for the rejection of some KOI planetary candidates. Some KOIs have low DSP either due to over correction of our light curves or light curves with high noise level. There are also 40 KOI planet candidates with BLS peaks selected by our pipeline but rejected during visual inspection. From further investigation, we find that 32 of these rejected transit signals are not visible when folded with twice the detected periods, probably due to strong transit timing variations. A detailed detection report of all the KOIs is presented in Table 2. We do not model the KOIs unless the host stars are found to have other

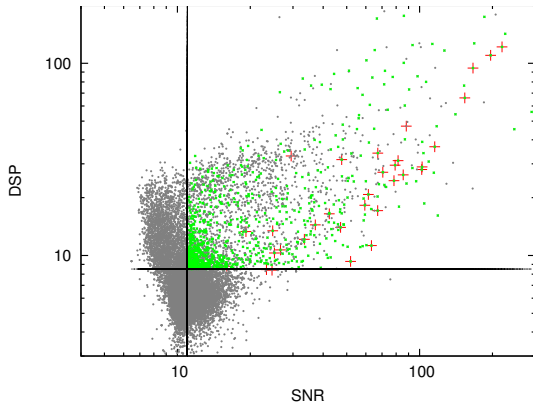


Figure 2. A demonstration of our selection methods. SNR versus DSP for all the first five BLS peaks from stars in sky groups 1, 12, and 19 (black dots). Solid lines present the lowest limit of SNR and DSP for selection. Green asterisks resemble all the BLS peaks actually selected for folding considering the period range and transit duration. Red crosses show the most significant peak of all the KOI planet candidates (34 in total) in these sky groups.

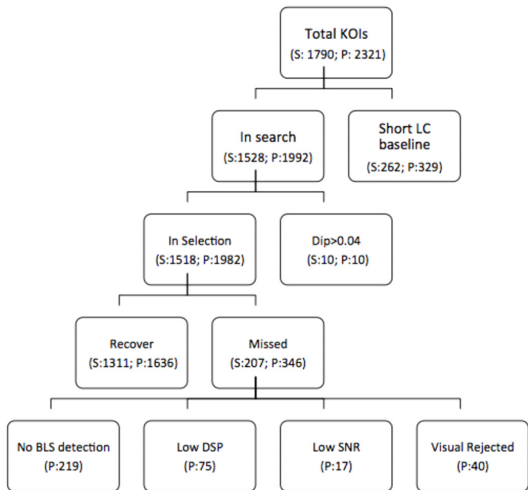


Figure 3. Summary of our recovery of KOIs in the B12 catalog. We show the number of stars (S) and planet candidates (P) in each category. The recovery rate of KOI host stars in our search range is 86.4%. The recovery rate of KOI planet candidates is 82.5%. For more information, see §3.1 and Table 2.

high SNR and DSP transit signals that are not reported by the Kepler team. The additional signals are treated as new candidates in our short list.

3.2 Generation of the planet candidate short list

We examined in detail the remaining candidates which are not included in the publicly available lists of candidates, EBs, or false positives (FPs). We re-applied the cosine filter to these light curves constructed with a greater number of cosine functions and a smaller frequency interval. We aimed to clean systematic variations from the light curves (whether intrinsic to the stars, or due to instrumental effects), leaving flat light curves with transits. The cosine functions are gen-

erated in a frequency range adjusted according to the visual determination of the frequency of the stellar variation. To preserve the transit signal, we applied a median filter with a window width at least twice that of the detected transit duration, before generating the cosine filter. BLS was applied again on the corrected light curves. The first ten peaks in the BLS spectrum are examined and compared to the previous detection, ensuring the detection of the transit signal is robust. As shown below in §3.3, all candidates were checked against false positive scenarios.

3.3 False positive detection and robustness checking

We use the moment-derived centroids provided by the *Kepler* FITS files to further eliminate possible FPs. For long period planet candidates, we visually examine the centroids at the transit time. For short period planet candidates, we examine the phase-folded centroid curves (de-trended by the cosine filter). We present one of our “failed” transit candidates as an example in Figure 4. The folded light curve would naively suggest that there is a transit signal due to a planet with $R_p/R_\star = 0.0198 \pm 0.0017$ and period of $P = 2.00783 \pm 3.8 \times 10^{-5}$ day. However, the phased centroids show a shift of ~ 0.004 pixels in the y direction during transit events, which indicates this is likely to be a false positive signal due to a blended eclipsing binary. According to the 2MASS image stamp, there is no nearby source within an area of $20'' \times 20''$, i.e. the binary is not resolved in the 2MASS images. We provide a list of forty false positives flagged by this method in Table 3. These stars have not been reported by the *Kepler* team in their false positive lists. They are also not reported as candidates by the *Kepler* team. The stellar information and estimated shifts in both directions are also given in our table.

We also used the public target pixel files and PyKE package⁶ developed by the *Kepler* team, to obtain pixel light curves for all of our candidates with transit depths greater than 1 mmag. It is difficult to perform the same analysis on shallower transits, because of the low signal-to-noise of the events in the light curves of individual pixels.

Here we take one of our new detections, KIC 005437945, as an example for our photometry analysis. We detected 4 non-periodic transit events altogether, which could be explained as due to two long period planet candidates with different epochs, depths and durations. The transits in Q1 and Q6 are due to a $P \approx 440$ days planet candidate; and the transits in Q2 and Q5 are due to a $P \approx 220$ days planet candidate (i.e. they are in a 2:1 resonance). We present the analysis for the transit event in Q6 here. We show the pixel image of out-of-transit, in-transit and the difference imaging in Figure 5. The images are computed by plotting the mean out-of-transit flux (± 2 day around the transit events), the mean in-transit flux and the difference between the two. The difference imaging during transit is identical to the out-of-transit flux distribution. No obvious background source is indicated for this particular star.

We further use the pixel calibration technique enabled by PyKE to extract light curves from every single pixel in

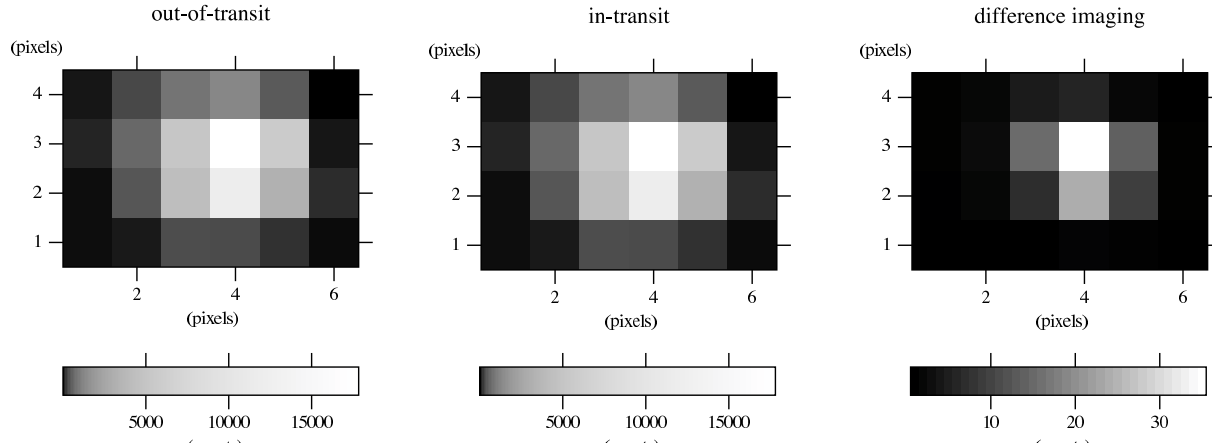


Figure 5. Out-of-transit image (in log scale of flux), in-transit image (in log scale of flux) and the difference between the two (in linear scale of flux) from the pixel files for KIC 005437945 Q6 transit. We do not see a visible shift in the flux distribution on the pixel image during transit, demonstrating that the apparent transit is not due to a variation of a background source.

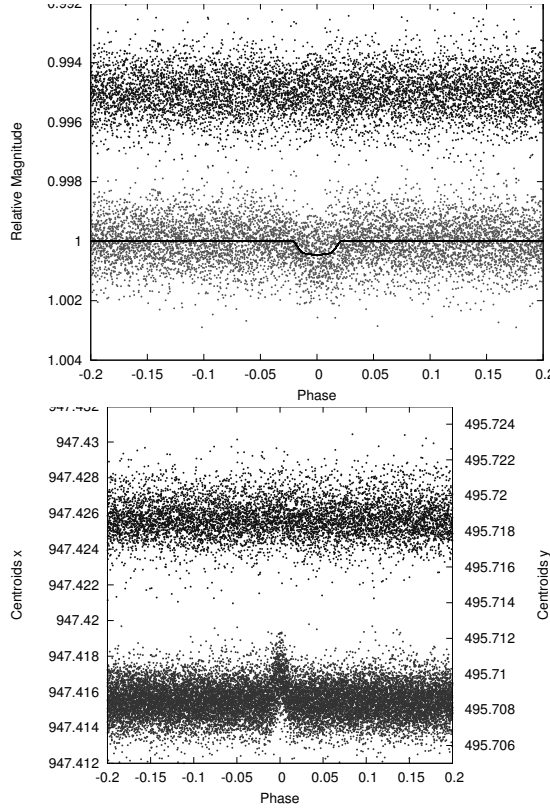


Figure 4. Light curves and centroids for KIC 004072333, phase-folded using the detected period and epoch. Top panel: phase-folded light curve (bottom) with period $P = 2.00783$ days and $E = 2455302.8774$ (BJD) and its residual from the fitting (top). Bottom panel: folded centroids in the x direction (top and grey) and the y direction (bottom and dark) with the same parameters. This detection is flagged as a false positive due to the shift of centroids in the y direction during transit. There is no visible companion in the 2MASS image stamp within $20'' \times 20''$ for this particular star.

the aperture. Figure 6 shows the light curves extracted separately from 6 pixels in the Q6 aperture (the aperture is shown in Figure 5). We can see that while the magnitude in every single pixel changes during the transit, they all show visible evidence for the transit event with roughly the same depth. The averaged flux from all the pixels has a flat out-of-transit magnitude. In addition, the centroids do not present an anomalous shift during the transit events.

For the rest of the transits which are not suitable for applying the single pixel analysis, we use other methods to at least ensure the robustness of the detection. We removed the detected transit signal according to the epoch, period and transit duration reported by BLS. Then we computed six different BLS spectra for each of the new light curves. The BLS spectra were obtained with 3 different sets of parameters (different frequency steps and bin numbers), each set of parameters are used twice. The first 10 peaks of every BLS spectrum were analyzed. We compared these 60 frequency peaks to our original transit detections. For all of the planetary transit signals we analyzed, the original periods as well as their harmonics were not detected in the transit-removed light curves.

Altogether 150 planet candidates entered our final list of new detections. The properties of their host stars are provided in Table 4. The detected periods range from ~ 0.17 day to ~ 440 days. We also found 6 new multiple systems (altogether with 15 planet candidates) in stars not in the B12 catalog. We found 57 new transit signals in KOI hosting stars; 43 of these are also independently reported by Ofir & Dreizler (2012, Hereafter O12). We also include 7 *single* transit events. One of these single transit events is around a KOI star with a known planet candidate. Using the convention of Batalha et al. (2012) for single transit events, we assign a negative integer period number for these potential candidates. We compute the minimum allowed period according to the given time span of the light curve and the epoch of transit. This is taken as the estimated period for single transit events in modeling.

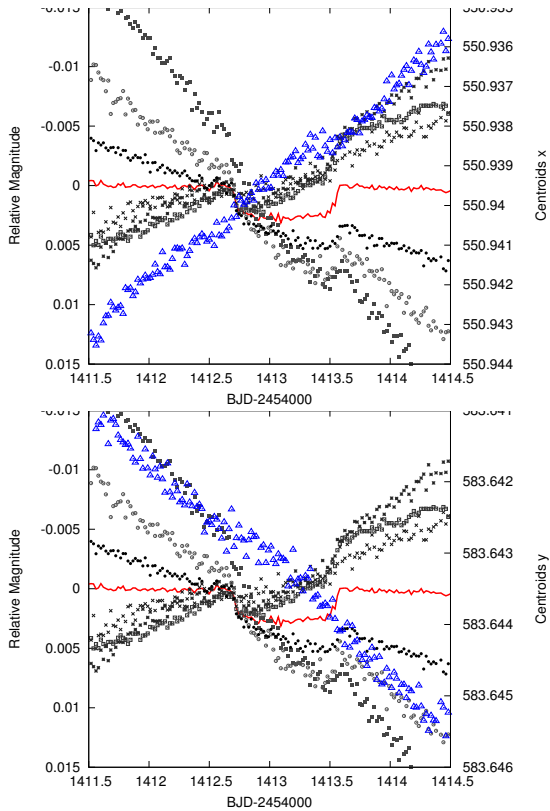


Figure 6. Red solid line: light curve flux for transit events in Q6 for KIC 005437945. Blue triangles: raw centroids x (top panel) and y (bottom panel). Different types of black points: light curves generated from different pixels separately in the aperture using `kepxtract` from the PyKE package.

3.4 Analysis

The transit modeling of all the candidates is based only on the *Kepler* light curves and the stellar parameters provided by the KIC. The parameters we can obtain directly from light curves are the transit depths, durations, ingress/egress durations, and individual transit centers.

Without radial velocity (RV) data, mass determinations for these systems are generally not available. It may be possible to measure the masses through subtle photometric effects, like ellipsoidal variations and relativistic beaming (Mazeh & Faigler 2010; Kipping & Spiegel 2011). These effects are prominent for close binary stellar systems as well as massive planet companions (Loeb & Gaudi 2003). We did not observe these effects in our candidates.

The eccentricity is also unknown, although broad limits can be placed on the orbital configuration for very wide transits (Kipping 2008). An eccentric orbit could result in asymmetry in the transit light curves, as well as a shift in the mid-time of transits relative to the occultation events. In principle, the eccentricity could also be derived from modeling the detailed shape of a transit light curve. However, detecting these effects requires extremely high resolution and SNR light curves, which were not available for our candidates. Generally speaking, we observe no apparent asymmetry in any of our candidates, which suggests modest eccentricity or certain values of argument of periastron. We assume circular orbits in our modeling, following the con-

vention of previous KOI modeling with only transit light curve information (Batalha et al. 2012).

We assume no flux dilution from blended nearby stars in our modeling. This is plausible for most of our candidates. We inspect the 2MASS image stamps with an area of $20'' \times 20''$ centered on each target. Four of them have nearby companions, which are marked out in Table 5.

In theory, one could also fit for the limb darkening coefficients, but this requires very high signal-to-noise and well sampled data, i.e. deep transits or many transit events (Kipping & Bakos 2011). We use a quadratic limb darkening formalism to model the transit light curves. The limb darkening coefficients (LDC) corresponding to the stellar atmospheres are interpolated with the stellar parameters from KIC in the ATLAS model grid LDCs provided by Sing (2010) for *Kepler*. The stellar parameters and the LDCs for the candidates are listed in Table 4. We also generate a grid of 1000 randomly selected stars from KIC with known stellar parameters and the interpolated their LDCs following the method described above. We then use these to determine LDCs for stars without information such as T_{eff} , $\log g$ and $[\text{Fe}/\text{H}]$ by linear interpolating in the J, H, K color space. Since the LDCs obtained with this method have larger uncertainties, the derived planet parameters for planets without host star parameters provided by KIC should be treated with caution.

To conclude, in our transit modeling, we *do not* fit for:

- the planet mass M_p ;
- the eccentricity e of the orbit, which is assumed to be zero;
- the blending due to nearby stars, which is set to be zero;
- the LDCs of stars, which are computed as described above.

We did fit the following geometric parameters which correspond:

- the fractional planet radius R_p/R_* ;
- the square of the impact parameter square b^2 ;
- the inverse of half duration $\zeta/R_* = 2/T_{\text{dur}}$. This quantity is related to a/R_* for zero eccentricity via the relation:

$$\frac{\zeta}{R_*} = \frac{a}{R_*} \frac{2\pi}{P} \frac{1}{\sqrt{1-b^2}}. \quad (2)$$

In the fitting procedure we constrained the quantities $b^2, R_p/R_*, \zeta/R_*$ to be the same for each individual transit for a selected candidate.

We also fitted for the additional parameters of out-of-transit magnitudes and transit centers. For the short period cases (with a period shorter than 30 days), we fit the median out-of-transit magnitude, first transit center T_A and the last transit center T_B as free parameters, with the total number of transits N fixed. We also assume that the transits are strictly periodic. We do not model the out-of-transit variation; the light curve is assumed to be flat. For our long period candidates, we use a slightly different method. We take the out-of-transit magnitude and transit centers of individual transits as independent parameters, the total number of free parameters in the fit for a transit light curve with N transits is $2N+3$. The periods of the candidates with only a single transit were estimated by the stellar density through KIC parameters, and by assuming no limb darkening and circular orbits (Yee & Gaudi 2008). The estimated periods for these cases are shorter than the lower limit constrained by the fact that only one transit event was observed during

Q1-Q6. These single events were fitted as if they were an individual transit in a long period system with a rough lower limit on the period.

In the fitting we used the formalism of Mandel & Agol (2002), and the methodology laid out in the analysis of HAT-Net planet discoveries (Bakos et al. 2010). A 10000 step Markov Chain Monte Carlo (MCMC) simulation is then applied around the best fitting parameters to explore the parameter space. The final reported planet parameters and estimated errors are taken as the median and median deviation of all the accepted jumps in the chain. The period is then recalculated by taking the median of $(T_B - T_A)/N$ for all the accepted jumps in the chain. We derive the transit number closest to the average of T_A and T_B (weighted by their errors as derived from the MCMC runs), and use the transit center of this event (calculated from T_A , T_B , N) as the optimal epoch.

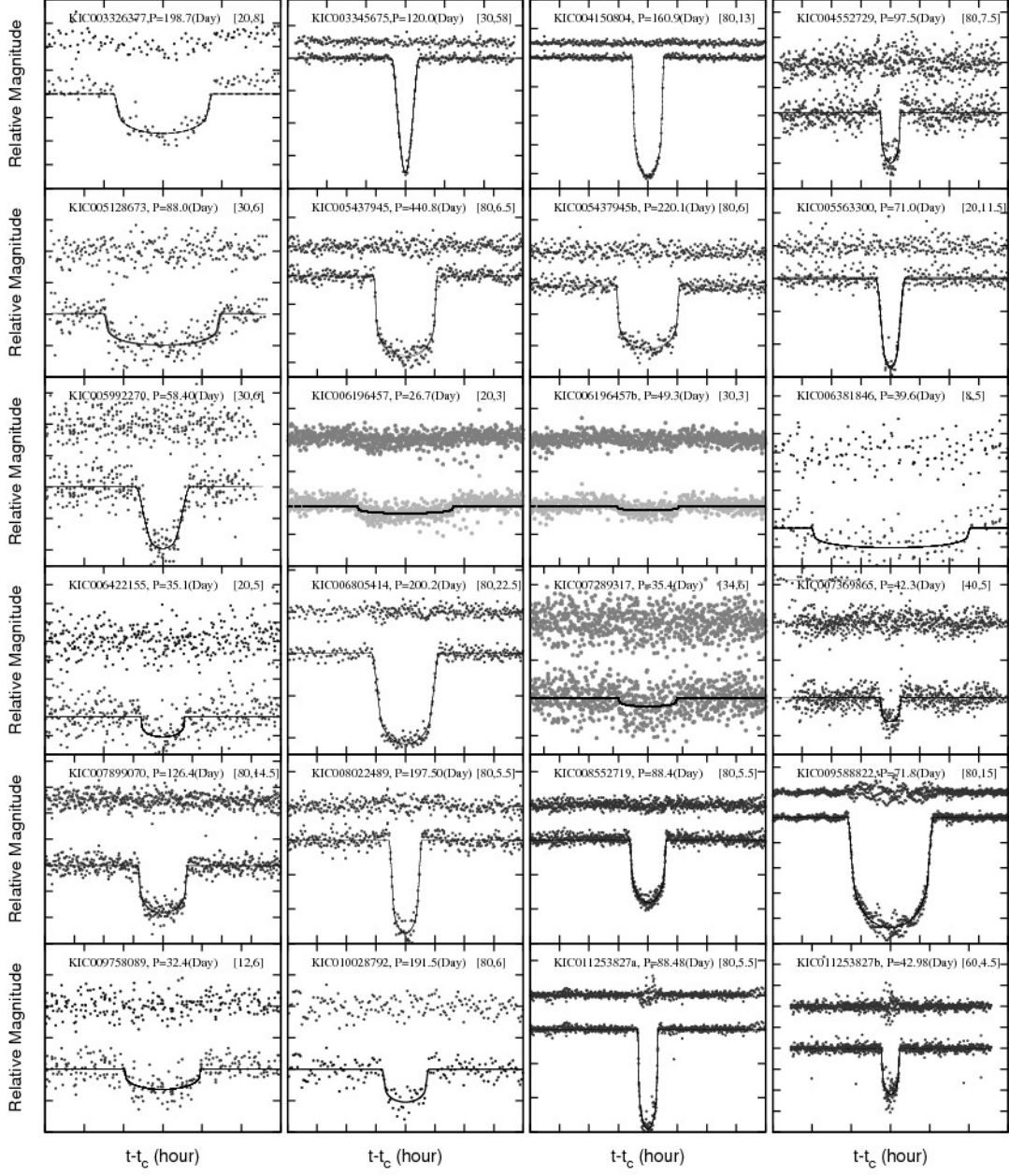


Figure 7. New Long Period planet candidates. For each candidate we show the best-fit model on the phase-folded light curve (bottom of the panel) and the residuals (top of the panel). For each candidate, we model all transits separately. We then fold the transits using the locally computed transit centers. We show the KIC number, period and scales of the figure of every planet candidate at the top of the subfigures. The x, y scales of the subfigure size are marked on the top right, in the units of [hours,1mmag].

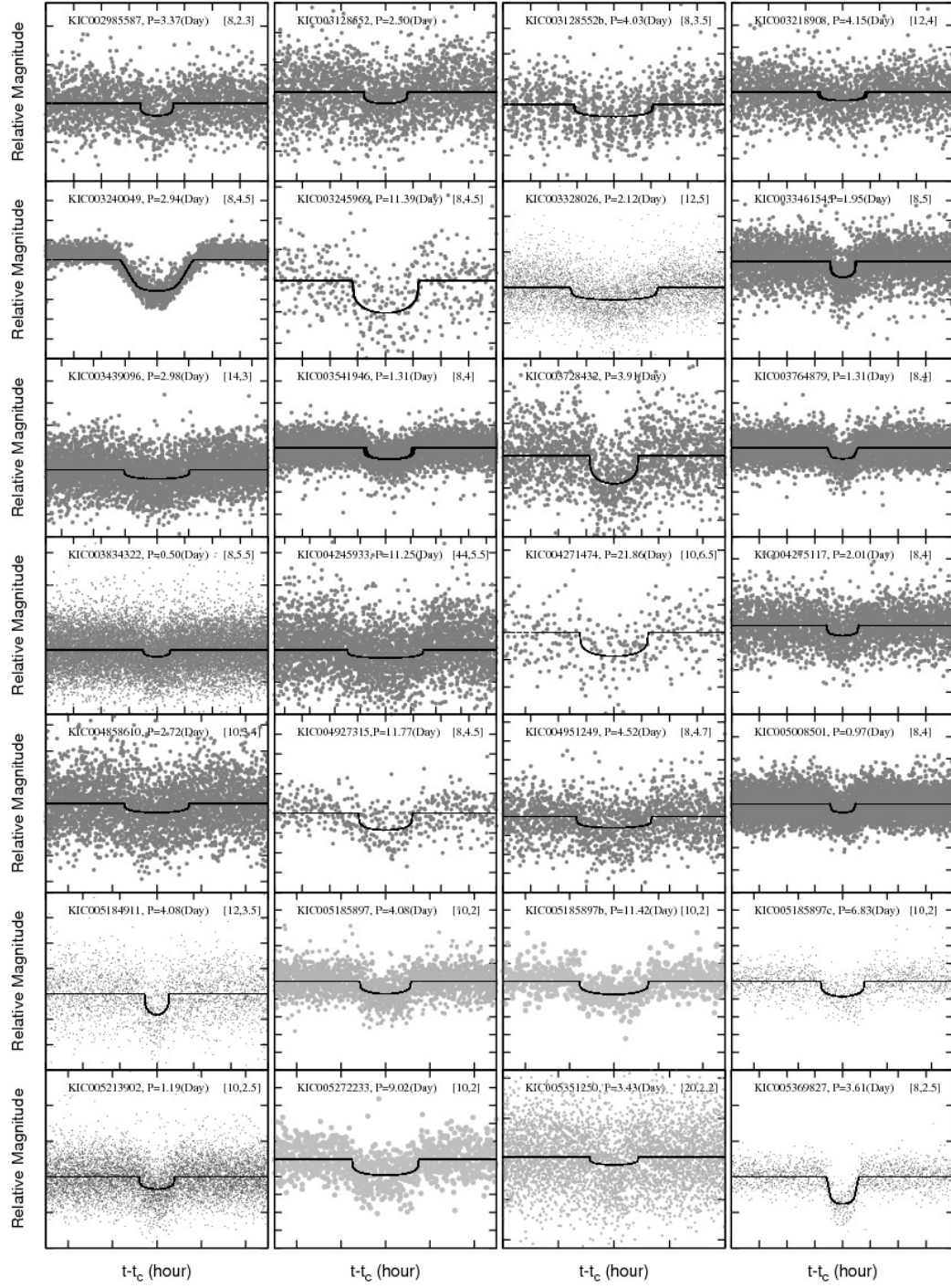


Figure 8. (a)

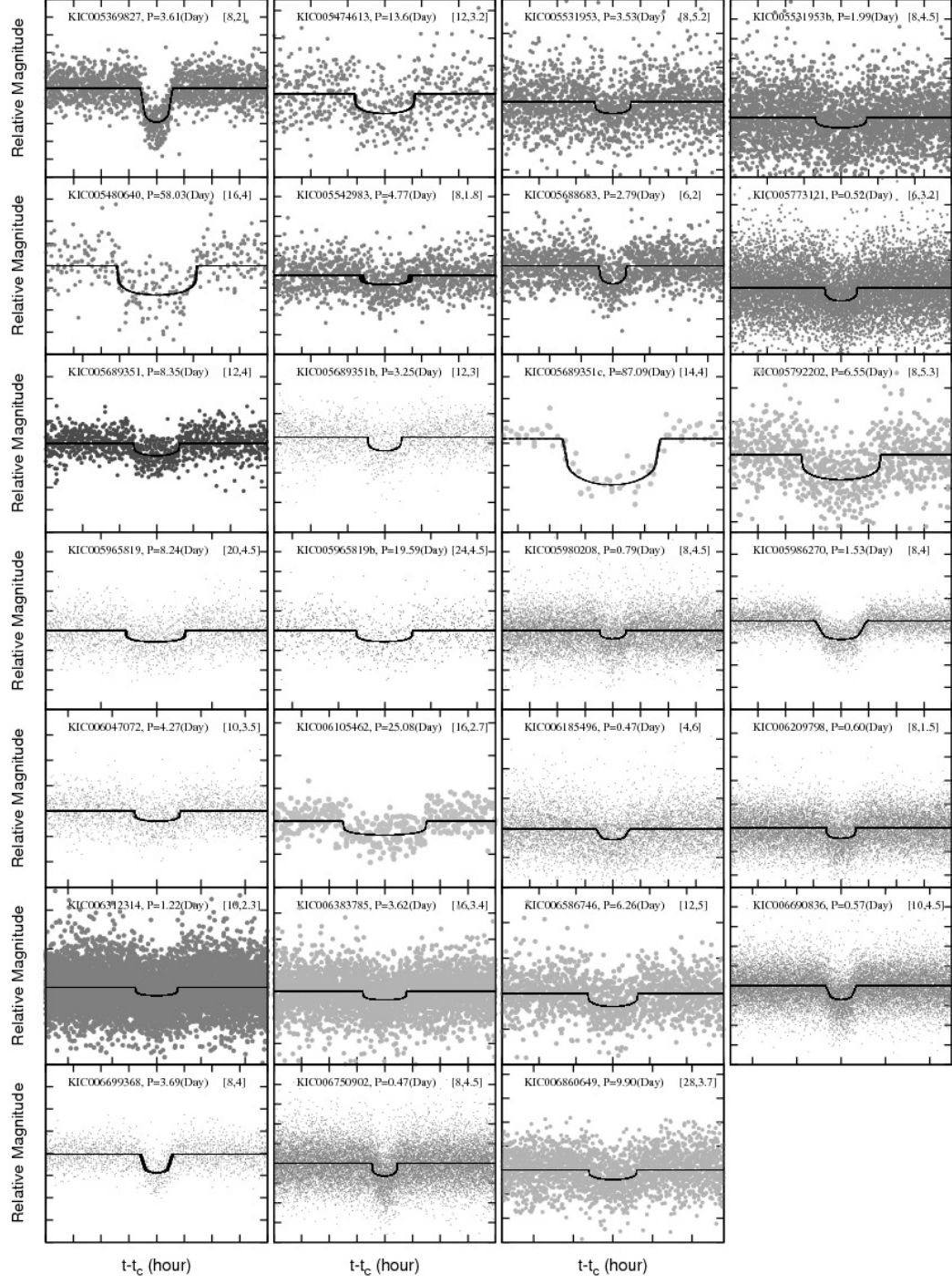


Figure 8. (b)

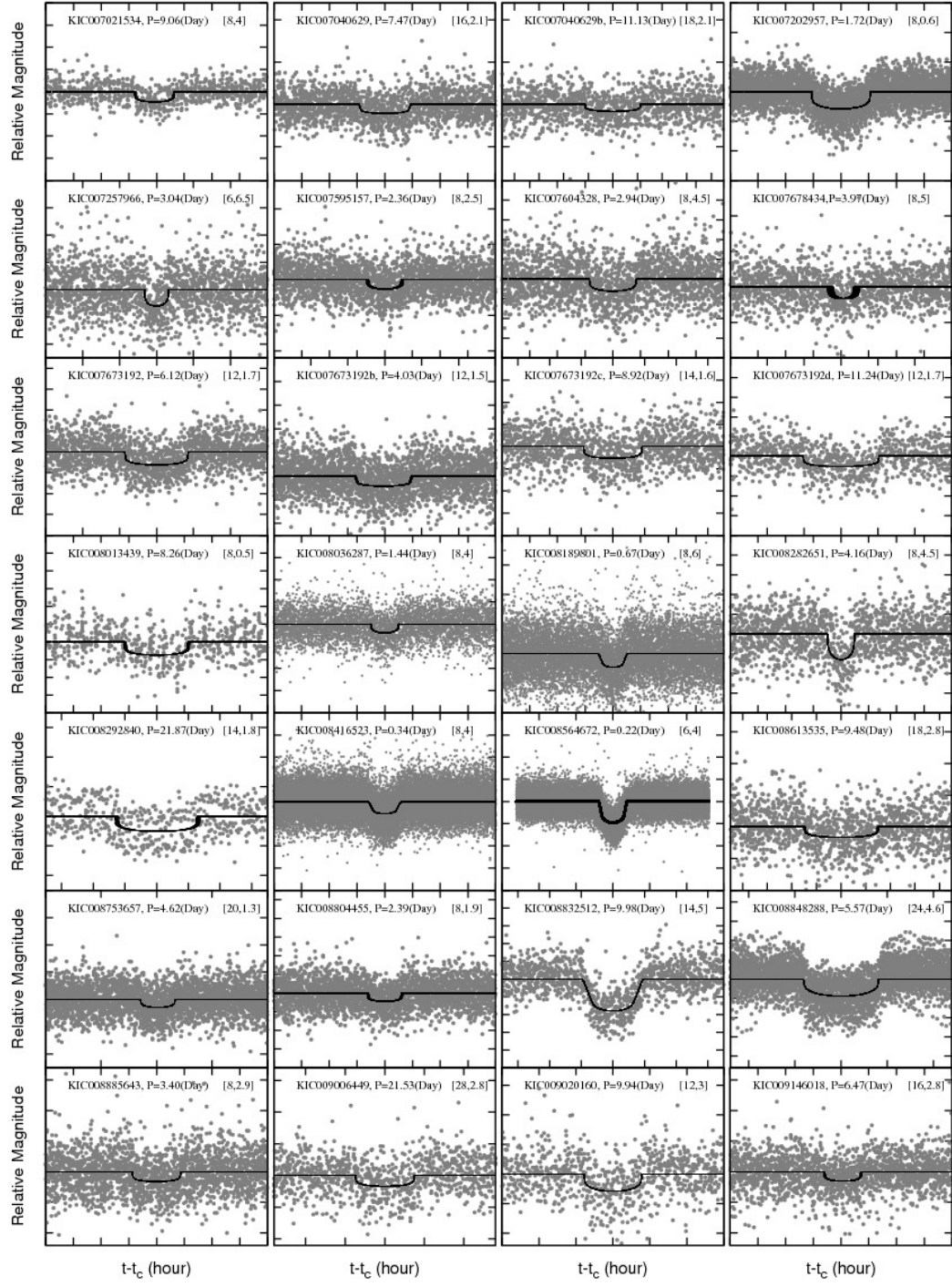


Figure 8. (c)

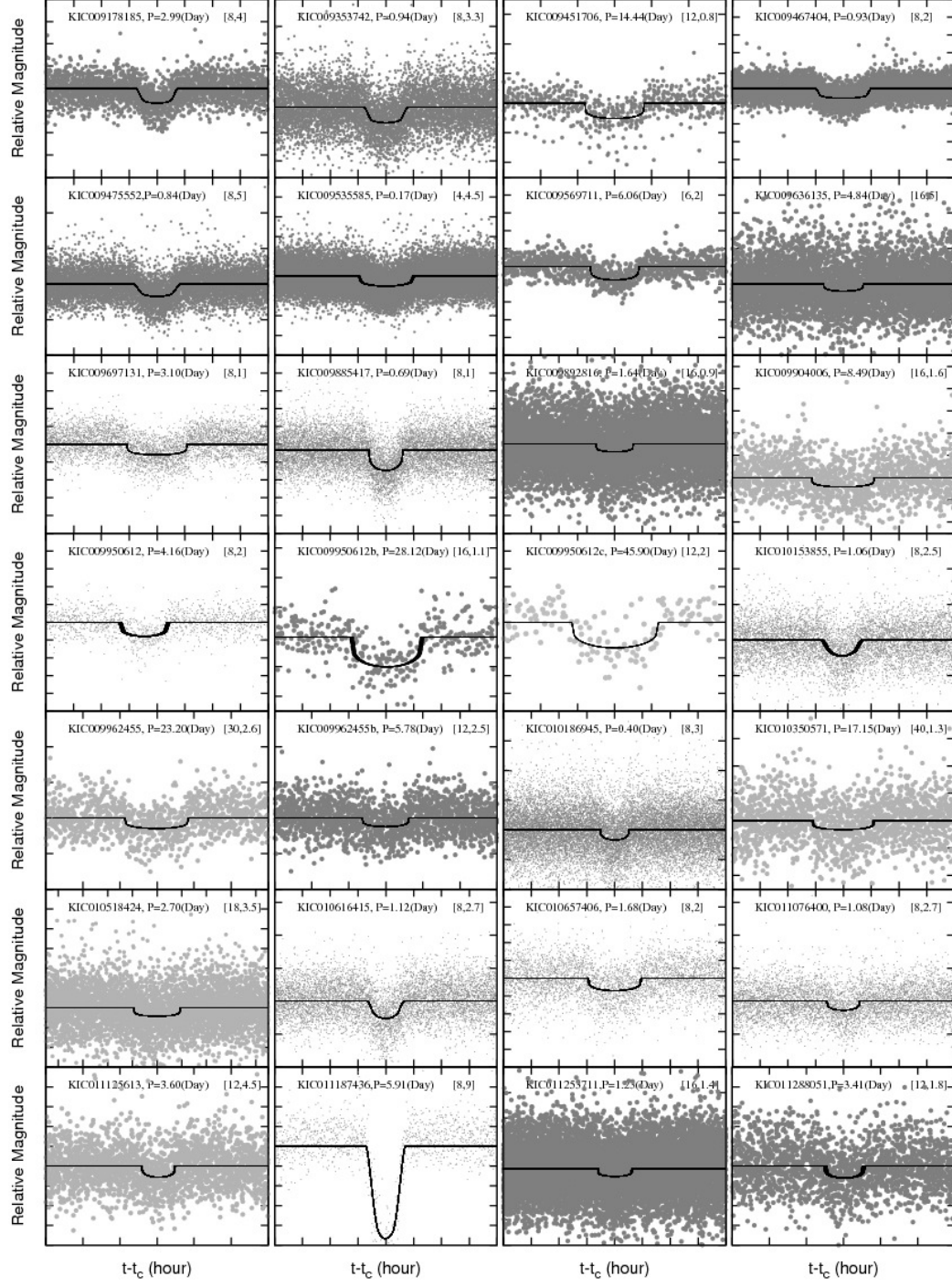


Figure 8. (d)

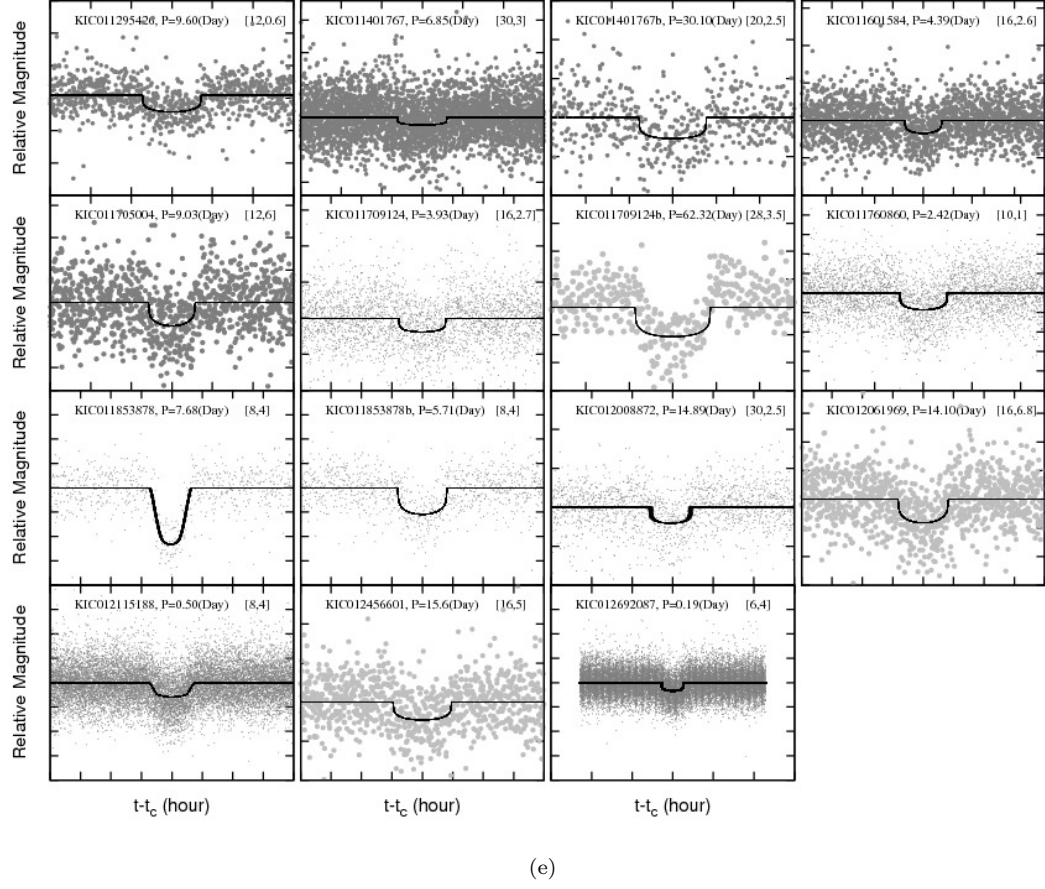


Figure 8. Short period planet candidates. For each candidate we show the best-fit model on the phase-folded light curve. The residuals are flat so we don't show them in the figures. The x, y scales of the subfigure size are marked on the top right, in the units of [hours, 1mmag].

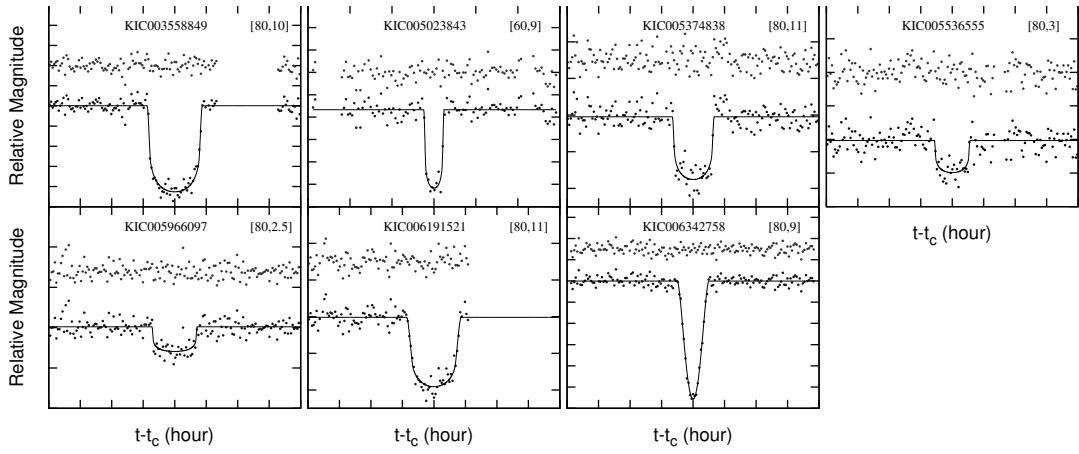


Figure 9. Single transit events. For each candidate we show the best-fit model on the light curve, together with the residuals from the fit (the configuration is the same as in Figure 7). The x, y scales of the subfigure size are marked on the top right, in the units of [hours, 1mmag].

3.5 Properties of candidates

We summarize the planet parameters for all the candidates in Table 5. The best fitted model on the phase folded light curves and the residuals from the best fitted model are presented in Figures 7, 8 and 9 for long period, short period and single transit planet candidates.

We compare the planet candidates reported in this paper with the B12 catalog KOIs in Figure 10. Our new planet candidates follow a similar distribution in the SNR and DSP space as the KOIs. This demonstrates that our recovery of new candidates is due to the efficiency of our pipeline rather than due to a reduction in the selection thresholds. We also show in the right of Figure 10 that the majority of new candidates have short period (less than 10 days) and small transit depth. For comparison, we plot the KOIs missed by our search in green, suggesting that our detection sensitivity drops as the period of the transit signal increases.

We plot the period and planet radius (in units of host star radii) histogram in Figure 11. The turn over points in both the period and radius space are modified with the supplementation of our new candidates. We suggest that our methods are more sensitive to short period candidates since the detection efficiency of BLS is generally higher in high frequency. We also confirm that the KOI samples are almost complete in the mid-period range. We do not have much advantage in the long period range over the original Kepler pipeline. The sample size around $P \sim 100$ days slightly gains with our new candidates. Signals with periods longer than 100 days usually suffer from over-correction of individual transit or low DSP simply because of lack of points in the transit phase.

Finally, we provide remarks on some of the interesting systems below⁷.

KIC 005185897: We found three planet candidates in the system, all with transit depths ~ 0.1 mmag. The periods of the candidates are 4.08 days (a), 11.42 days (b) and 6.83 days (c). (See Figure 8 (a), row 6, column 2, 3 and 4.) The stellar radius from KIC is only $0.51 R_\odot$, which makes the modelled radii extremely small for all the candidates in the system. The $P = 11.42$ day signal and 4.08 day signal are modelled to be $\sim 0.62 R_\oplus$, and the 6.83 days signal is slightly larger ($0.67 R_\oplus$). They are also the smallest planet candidates we found around non-KOI stars. Both the pair b and c, c and a are around 5:3 resonance. The planet candidate (a) was also found by the TPS algorithm as a potential transit signal (T12).

KIC 005437945: We identify four transit events in the light curve. The transit events in Q1 and Q6, and the ones in Q2 and Q5 share the same depths and durations, respectively. The former is modelled to be a $7.5 R_\oplus$ planet candidates with 440 day period; the latter is modelled to be a $6.4 R_\oplus$ planet candidate with a period of 220 days. (See Figure 7, row 2, column 2 and 3.) We note that the transit in Q1 is independently identified and classified as a single transit event by the Planet Hunters (Schwamb et al. 2012). A tweak happened during the transit in Q2 for the inner planet candidate; by carefully offsetting the magnitude on

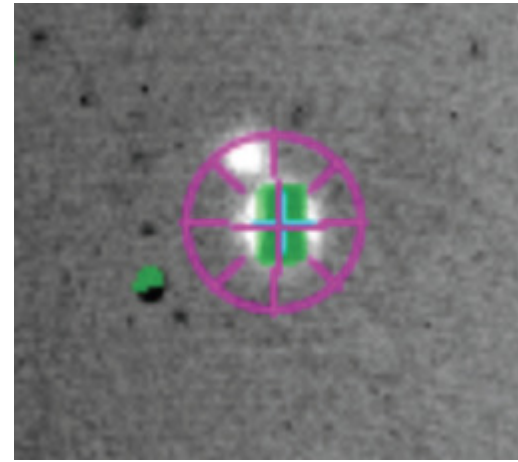


Figure 12. Image of the star KIC 5437945 taken with the APO 3.5 m Echelle slitviewer. The guider is centered on the star. A companion is resolved within $\sim 5''$.

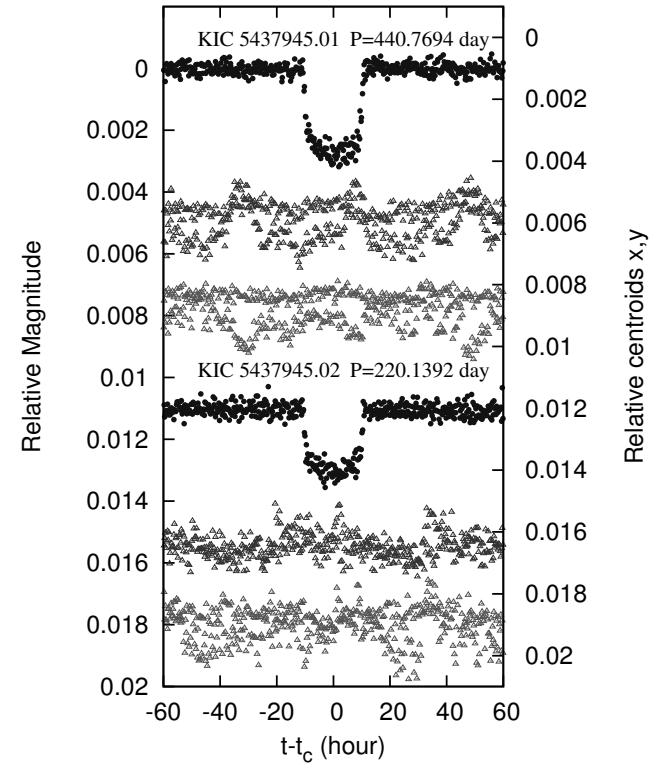


Figure 13. The two planet candidates of star KIC 5437945: from black to grey are the phased folded light curve, and the phased folded x and y direction centroids, all displayed separately. The upper (lower) three plots are for the first (second) planet candidate, with period $P \sim 440(220)$ day. The centroids in the figure are the mean centroids after de-trending.

⁷ The planet and stellar parameters we quote here are only approximated numbers for easy comparison. For accurate parameters and estimated errors, refer to Table 5.

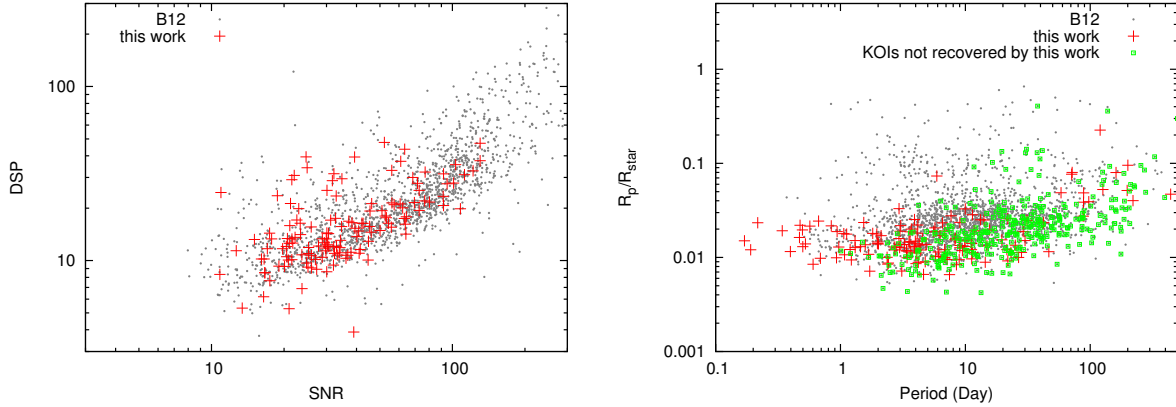


Figure 10. Comparison of KOIs and the planet candidates reported in this paper. Left: in SNR-DSP space; Right: in period-transit depth space. The black dots represents all the KOI planet candidates. The red cross represents the new candidates in this paper. In the right figure, the green squares show the KOIs missed by our searching process.

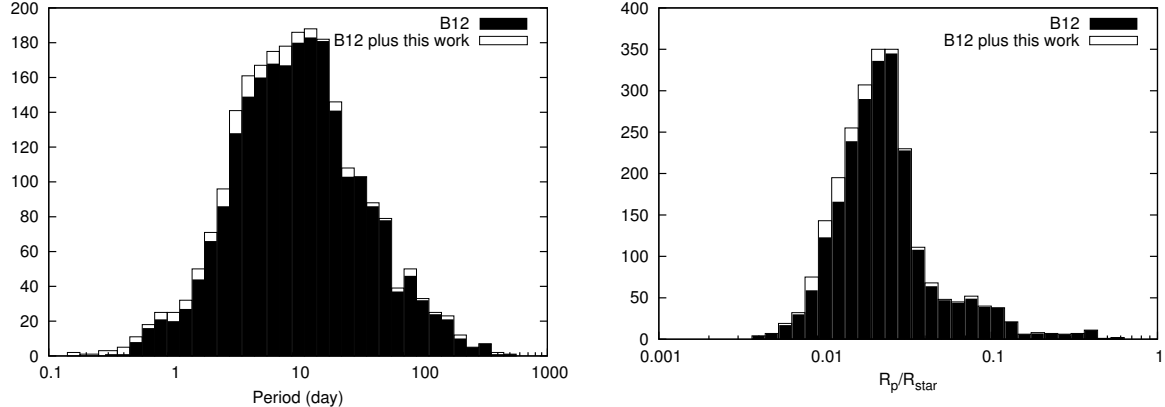


Figure 11. Comparison of the distribution of periods (left) and R_p/R_{star} (right) between KOIs and the total (KOIs and this work). The shadowed regions is the distribution from KOI planet candidates alone.

both sides of the tweak, we recover the full transit signal. We resolved a faint close companion ($\sim 5''$) in the Echelle slitviewer of the APO 3.5 m telescope (See Figure 12). We examined 2MASS image stamps in J,H and K and DSS 1,2 images in red and blue. All of the above show that the companion is bluer than KIC 005437945, which indicates that it is unlikely to be a physically associated companion. We present the phase folded de-trended centroid for both planet candidates in Figure 13. No anomalous motion is shown in either direction during transit.

KIC 005965819: We found two planet candidates in the system, both with modelled radii less than $2 R_{\oplus}$. The inner planet candidate orbits the host star with a period of 8.2 days; the outer planet candidate has a 19.6 day period. (See Figure 8 (b), row 3, column 1 and 2.) They are not in a tight resonance with each other. We note that the transit durations of these two planet candidates are longer than the values expected assuming circular orbits. This might indicate that the planets are in eccentric orbits or the stellar radius of KIC 005965819 is in fact larger than what is listed in the KIC.

KIC 007673192: We found four planet candidates in the system, all with modelled radii around $1 R_{\oplus}$. The periods

of the candidates are 6.12 days (a), 4.03 days (b), 8.92 days (c) and 11.24 days (d). (See Figure 8 (c), row 3.) They are not around any low order resonance pairs. T12 also identified the $P=6.12$ day signal as a potential transit signal.

KIC 009962455: We found two planet candidates in the system, both with modelled radii around $1 R_{\oplus}$. The periods of the candidates are 23.20 days (a), 5.78 days (b), in 4:1 resonance. (See Figure 8 (d), row 5, column 2 and 3.) The 23.20 day component in the system was also found by T12.

KIC 009535585: The shortest period candidate we found. The signal is modelled as a $1.6 R_{\oplus}$ super earth with a period of only 0.17 day. (See Figure 8(d), row 2, column 2.) If this candidate is confirmed, it would hold the record of the shortest period among the KOIs.

KIC 011253827: We found two planet candidates in the system. The outer planet is Saturn-like with a radius of $6.18 R_{\oplus}$ and period of ~ 88 days. The inner planet is $\sim 3.82 R_{\oplus}$ with a 43 days period. (See Figure 7, row 6, column 3 and 4.) The Planet Hunters independently found these signals in their web discussion.

KIC 012692087: Also a extremely short period candi-

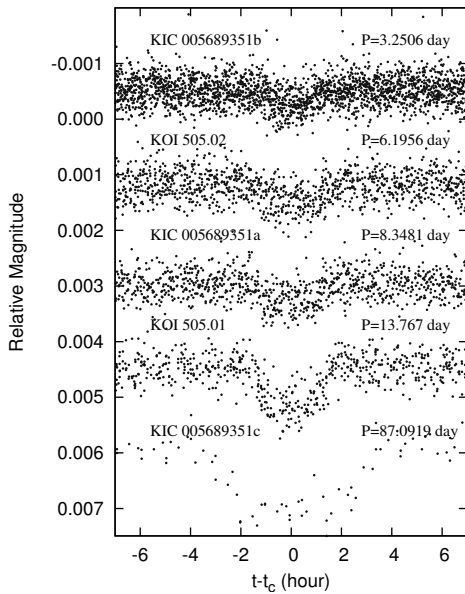


Figure 14. Folded de-trended light curve of KIC 005689351. Each transit is folded relative to its measured epoch, with the signal corresponding to the other planet candidates removed from the light curve. From top to bottom, the periods of the planet candidates are 3.25 days, 6.20 days, 8.35 days, 13.77 days and 87.09 days, respectively. The candidates with periods of 13.77 days and 6.20 days have already been identified as KOI 505.01 and KOI 505.02.

date, really similar to KIC 009535585, with 0.19 day period and $1.5 R_{\oplus}$ radii. (See Figure 8(e), row 4, column 3.)

KIC 005689351 (KOI 505): A rich system with potentially as many as 3 more planet candidates. We initially identified a $2.2 R_{\oplus}$ planet candidate with a period of 8.348 (a) day in the system, which already has 2 KOIs. While this paper was under revision, O12 pointed out that there might be 2 additional signals in the system, with periods of 3.25 days (b) and 87.09 (c) days. (See Figure 8 (b), row 3, column 1, 2, 3.) We find the same signals in this light curve after reprocessing the data. The folded light curve of the three planet candidates are separately shown in Figure 14. When modeling one planet candidate, we make use of the detected periods and epochs to filter out the transit signals due to the other two. The top and middle panels present the two KOIs, with periods of 13.767 days and 6.1956 days. The third planet candidate we found is in a 4:3 resonance with the latter. This is the first reported 3:4:6 resonance 3-planet candidate system. Rein et al. (2012) suggests that a resonance chain of three or more planets, in analog to Jupiter's moon system, would overcome the difficulties of forming the 4:3 resonance in the traditional way. This system provides an interesting testing-ground for the theory.

KIC 007595157 (KOI 246): A sub-earth candidate with $0.64 R_{\oplus}$ orbiting the star with a period of ~ 2.4 days. (See Figure 8 (c), row 2, column 2.) It was a single planetary system in B12 catalog, with KOI 246.01 ($1.3 R_{\oplus}$ radii and 3.4 days period).

KIC 008753657 (KOI 321): A candidate hot Mars, also the smallest candidate from our new findings, with a modelled radius of $0.5 R_{\oplus}$ and period of 4.6 days. (See Figure 8 (c), row 6, column 1.) This is also reported by the Ofir team

(O12) with similar modelled parameters. The system was previously known to host KOI 321.01, a 2.4 days candidate superearth.

KIC 11295426 (KOI 246): B12 catalog found it to host a superearth (KOI 246.01) with a 5.38 days period. We found an outer planet candidate with $0.58 R_{\oplus}$ radii and 9.6 day period. (See Figure 8 (e), row 1, column 1.) This is also reported by O12.

4 CONCLUSIONS

We have analyzed 124840 stars with public *Kepler* data from quarters Q1–Q6 in total. The large majority of our candidates have already been identified by the *Kepler* team. We recover 92% of Kepler findings from the B11 catalog and the majority (86.4% of the planet hosting stars and 82.5% of the planet candidates) of the B12 catalog. Forty new false positives are identified in our analysis of centroids variation. We report 150 new planet candidates and 7 *single* transit events that haven't been assigned as KOIs (Kepler Objects of Interests) in this blind search. 55 of these planet candidates are listed as potential transit signals by the automatic TPS algorithm developed by the *Kepler* team (T12). While this paper was under revision, O12 conducted a search of new planet candidates using the SARS pipeline in all the KOIs, 43 of the planet candidates in this work overlap with their findings. To our best knowledge, 22 of these planet candidates and 3 of the single transits are also independently identified by the Planet Hunters in their public website discussion session. 40 of the planet candidates and 4 of the single transits are reported for the first time.

The periods of our new candidates range from ~ 0.17 days to $\gtrsim 440$ days. The estimated planetary radii vary from $\sim 0.5 R_{\oplus}$ to $62 R_{\oplus}$. 124 of the planet candidates and three of the single transits have sizes smaller than $3 R_{\oplus}$. We also found 6 new candidate multiple systems. In addition, we found 57 more planet candidates in the already known KOI systems. By comparing our new findings with the Kepler candidates, it appears that for short periods (< 10 day), our pipeline and search procedure finds somewhat more candidates than the Kepler pipeline. Most of the *single* transit events (and a few of the planet candidates) were found by visual inspection of the light curves that were flagged by BLS. This suggests that combining automated searches, and visual inspection is an efficient approach for transiting planet searches. Our searching process could potentially act as a supplementation of the findings from the Kepler team to improve the statistics in the short period planets. We trust that independent searches will be benefit both the Kepler team and the community.

Table 1. Anomaly Summary Table

Start(BJD-2454000)	End(BJD-2454000)	Quarter	Anomaly Type
1002.5198	1002.7241	2	EXCLUDE ^a
1014.5146	1016.7214	2	SAFE MODE ^b
1033.2932	1033.3341	2	TWEAK ^c
1056.4853	1056.8313	2	COARSE POINT ^d
1063.2896	1064.3726	2	EARTH POINT ^e
1073.3632	1073.3632	2	ARGABRIGHTENING ^f
1079.1866	1079.1866	2	TWEAK
1080.8008	1080.8212	2	ARGABRIGHTENING
1088.4018	1089.3213	2	COARSE POINT
1093.2239	1093.2239	3	EARTH POINT
1100.4163	1100.5389	3	COARSE POINT
1104.5233	1104.5438	3	COARSE POINT
1113.4116	1117.3346	3	MEMORY ERROR ^g
1123.5461	1124.4248	3	EARTH POINT
1206.2584	1206.2584	4	TWEAK
1216.4137	1217.3128	4	EARTH POINT
1229.8386	1233.8231	4	SAFE MODE
1307.9995	1309.2869	5	-
1336.7713	1337.6091	5	-
1399.5042	1400.3828	6	EARTH POINT
1431.2374	1432.1978	6	EARTH POINT

^a EXCLUDE: manually excluded cadence before pipeline processing.

^b SAFE MODE: due to unanticipated sensitivity to cosmic radiation, or unanticipated responses to command sequences. The amplitude of flux is affected after the end date of safe mode, data for additional 3 days are removed rather than corrected. Data on both side are offset in magnitude to ensure continuity by a polynomial fit.

^c TWEAK (Attitude Tweaks): discontinuities in the data due to small attitude adjustments. The discontinuities are corrected by offseting the data on both sides using a polynomial fit.

^d COARSE POINT (Loss of Fine Pointing): due to losing fine pointing control, removed.

^e EARTH POINT: change of attitude due to monthly data downlink. Affect data the same way as safe mode. Corrected by the same method as safe mode.

^f ARGABRIGHTENING: diffuse illumination of the focal plane. Removed. Only argabrightening events longer than one cadence are listed here.

^g MEMORY ERROR: due to onboard spacecraft errors, gapped by the pipeline, the continuity on both ends of a gap is checked. Only a single memory error longer than one cadence is listed here.

^h The format of data release handbook 8 for Q5 data is different from other quarters. There are no safe mode, tweak, coarse point or exclude phenomena in Q5, only two big gaps, possibly due to earth point, are listed.

Table 2. Detection report of KOIs^h

KOI	KIC	Kepperiod day	period day	Kepepoch BJD-2454000	epoch BJD-2454000	dip magnitude	Q ⁱ	SNR	DSP	COMMENTS
1.01	11446443	2.470613	955.76257	-	6.10e-03	7.55e-02	-	-	-	sod ^a
2.01	10666592	2.204735	2.204760	954.35780	965.37828	-	-	206.05	179.41	
3.01	10748390	4.887800	4.887970	957.81254	967.579324	2.60e-03	2.39e-02	439.78	55.43	wp ^b
157.04	6541920	46.687100	22.689217	-	981.433477	6.00e-04	1.11e-02	58.68	37.10	wp
157.05	6541920	118.363800	113.449430	-	1026.812678	8.00e-04	2.10e-03	15.36	21.01	snd ^c
375.01	12356617	600.000000	-	1072.22382	-	-	-	-	-	
1099.01	2853093	161.526600	-	1031.00152	-	-	-	32.38	5.94	ld ^d
1448.01	9705459	2.486600	2.486616	967.10929	964.62009	4.25e-02	4.46e-02	167.96	135.49	lr ^e
1888.01	100633802	120.019000	-	967.18256	-	-	-	10.05	13.06	ls ^f
2066.01	3239671	147.972400	-	1096.09006	-	-	-	-1.00	-1.00	nd ^g
...

^a sod (short of data): KOIs don't have sufficient length of long cadence data to fulfill the requirement of TFA. They are not selected for our reanalysis.

^b wp (wrong period): KOIs recovered with a wrong period. For some planet candidates, the harmonics of the KOI period (or other periods due to the imperfect correction of the light curve) show higher SNR and DSP in the BLS analysis. The SNR and DSP value reported here corresponds to the detected signal instead of the KOI period. In other cases, frequencies not related to the signal are detected, the true signal is recovered in visual inspection, we fill the SNR and DSP with '-'.

^c snd (single transit, no detection): KOIs with a single transit, and all the reported BLS peaks are under our selection limits.

^d ld (low DSP): KOIs with lower DSP than our selection limits, therefore not recovered in our selection process.

^e lr (large radius): KOIs with transit dip larger than 0.04, therefore not selected for analysis.

^f ls (low SNR): KOIs with lower SNR than our selection limits, therefore not recovered in our selection process.

^g nd (no detection): KOIs for which the first five BLS peaks are under our selection limits, and the correct period is not one of the first five BLS peaks.

^h We compare the parameters of KOIs with the B12 catalog. The period, epoch, dip and q are taken from our BLS analysis instead of modeling the candidates. A complete version of this table can be accessed from the online version and download from <https://sites.google.com/site/largepunkenkelephant/tables>.

ⁱ Q: a dimensionless parameter representing the transit duration. Defined as T_{dur}/P .

Table 3. False Positive List

Star	Kepmag	RA (deg)	Dec (deg)	Epoch (BJD-2454000)	Period (day)	Displacement x ^b (Pixel)	Displacement y ^b (Pixel)	SNR
2442359	13.931	19 24 53.566	+37 46 53.58	965.8428	0.55283	-0.0025	-	26.16
3336765	13.617	19 19 49.397	+38 27 49.07	965.1613	1.84483	-	-0.00032	38.93
3852258	13.819	19 27 55.433	+38 58 16.25	968.1106	5.75838	-	0.005	17.48
4035667	10.035	18 58 29.566	+39 10 56.68	965.5837	2.87366	-0.007	0.005	-1.00
4072333	15.664	19 41 19.236	+39 09 45.14	965.5638	2.00775	-	0.0030	37.69
4077901	13.007	19 45 42.948	+39 08 01.54	967.7249	6.05444	+	0.002	27.22
4270565	15.154	19 34 24.946	+39 23 18.96	972.2024	18.01143	0.007	-0.007	28.47
5443775	12.936	19 21 20.671	+40 39 11.02	967.8765	3.30754	-	-0.00034	73.09
5565497 ^c	11.521	19 57 31.702	+40 45 29.30	966.11575	1.412532	-0.0126	-0.0011	131.4
5622812	12.832	19 30 41.270	+40 52 10.34	964.8384	0.10304	-0.005	-0.005	49.76
5649325 ^c	13.560	19 55 55.289	+40 52 19.34	1196.35	195.63	0.0016	-	7.81
...

^a We only report the false positives not in the *Kepler* FP catalog here. We do not report FPs in *single* transit events. These FPs are all identified by examining the centroids. We refer to the text for a detailed description of the method. A complete version of this table can be accessed from the online version and downloaded from <https://sites.google.com/site/largepunkelephant/tables>.

^b The flux centroid displacement amplitude is computed from the phase folded centroids. The x and y direction are listed separately. We do not list a displacement when the shift is not detected.

^c There are visible companion(s) in the 2MASS image stamp within 20" × 20".

Table 4. Stellar Parameter Table

Star	Kepmag	T_{eff} (R_{\odot})	$\log g$ (K)	[Fe/H] (cgs)	R_{\star}	u_a^{b}	u_b^{c}
2985587	13.910	6023	4.278	-0.069	1.276	0.34	0.29
3128552	14.523	5530	4.673	-0.248	0.761	0.41	0.25
3240049	11.557	4435	2.127	-0.065	17.188	0.65	0.09
3245969	15.681	4825	4.789	0.054	0.594	0.59	0.13
3328026	15.147	5681	4.508	0.147	0.947	0.42	0.24
3345675	15.635	4105	4.628	0.137	0.598	0.57	0.17
3346154	14.575	5513	4.490	0.118	0.957	0.45	0.22
3439096	13.799	4940	3.119	-0.340	5.493	0.52	0.18
3541946	13.597	5537	4.728	-0.140	0.711	0.43	0.24
3558849	14.218	5938	4.432	-0.410	1.052	0.33	0.30
3728432	15.646	4371	4.583	-0.254	0.696	0.59	0.13
3764879	14.024	5845	4.641	0.006	0.809	0.38	0.27
3834322	15.397	4627	4.631	-0.004	0.698	0.62	0.11
4150804 ^d	12.888	-	-	-	-	0.40	0.25
...

^a A complete version of this table can be accessed from the online version of the paper and downloaded from <https://sites.google.com/site/largepunkelephant/tables>.

^b The quadratic limb darkening parameter a.

^c The quadratic limb darkening parameter b.

^d The limb darkening coefficient is obtained from the estimated stellar properties based on the J, H and K magnitudes.

Table 5. Planet Candidates Table

KIC	Epoch (BJD-2454000)	σ_E (10^{-3})	Period (day)	σ_P (10^{-4})	R_p (R_\oplus)	R_p/R_*	σ_{R_*} (10^{-3})	b	ζ/R_* (day^{-1})	SNR	DSP	χ^2	Comments
2985587	1159.6256	1.5	3.375816	0.52	1.64040	0.01178	0.84	0.68 ± 0.19	42.99 ± 2.9	40.83	14.78	1.44	
3128552	1219.6102	1.2	2.504621	0.18	1.06137	0.01278	0.90	0.66 ± 0.19	24.26 ± 0.86	27.167	9.826	4.16	KOI2055, bO12 ^c
3128552	1298.5430	4.9	4.025928	0.75	1.1627	0.0140	1.1	0.68 ± 0.18	16.91 ± 0.50	33.43	10.76	4.16	KOI2055, O12
3218908	1187.6632	1.2	4.152573	0.54	0.9736	0.0128	0.96	0.64 ± 0.20	18.73 ± 0.61	27.1020	12.7280	4.09	KOI1108, O12
324049	1234.98694	0.43	2.9454270	0.094	61.9190	0.03301	0.99	0.95 ± 0.037	23.61 ± 0.33	24.94	34.13	0.62	T12 _d
3245969	1301.042	15	11.39060	1.8	1.8410	0.0284	1.9	0.46 ± 0.38	20.4 ± 1.7	36.80	10.72	18.97	KOI1101, T12
3326377	1188.2283	1.8	198.7039	20	3.7018	0.0379	1.8	0.67 ± 0.15	6.127 ± 0.080	19.5130	24.9130	3.22	KOI11830, O12
3328026	11102.5054	1.7	2.115515	0.39	1.75795	0.01701	0.73	0.58 ± 0.12	10.6 ± 1.1	103.06	35.56	6.96	T12 _e
3345675	1203.14403	0.12	120.002673	0.80	14.73987	0.02586	0.28	0.90 ± 0.02	26.70 ± 0.000	8.03	17.837	18.34	wp ^f , PHt ^f
3346154	1231.72962	0.31	1.927041	0.057	1.8555891	0.01777	0.78	0.48 ± 0.20	53.7 ± 1.1	105.71	22.92	4.40	T12
3439096	1108.8290	1.3	2.975892	0.21	7.61918	0.01271	0.50	0.53 ± 0.17	11.74 ± 0.21	32.91	23.49	3.71	
3541946	1270.418	12	1.311837	0.13	0.9854	0.0127	5.2	0.17 ± 0.83	20.6 ± 2.0	61.05	37.19	1.50	KOI624, O12
3558849	1112.9840	1.5	-258	-	6.67780	0.05817	0.61	0.34 ± 0.12	2.919 ± 0.013	-	-	2.11	
3728432	1314.79711	0.22	3.9086360	0.043	1.92017	0.02528	0.47	0.30 ± 0.14	27.83 ± 0.20	107.92	19.85	15.22	T12
3764879	1118.75219	0.68	1.3069750	0.067	1.33331	0.0151	1.0	0.73 ± 0.17	49.29 ± 1.80	112.23	31.15	1.69	T12
3834322	1.087.18555	0.12	0.49844300	0.0040	0.99103	0.01301	0.47	0.46 ± 0.16	50.41 ± 0.68	17.46	7.65	8.90	T12
4150804	1271.38683	0.69	160.8818	10	-	0.07985	0.64	0.365 ± 0.080	4.801 ± 0.13	12.06	24.85	0.35	PH ^f
4245933	1165.1932	1.9	11.25629	1.3	0.81285	0.01408	0.45	0.46 ± 0.17	3.23 ± 0.027	25.29	11.88	13.00	T12
4271474	1262.46308	0.40	21.86183	1.1	1.71411	0.02580	0.59	0.35 ± 0.14	15.71 ± 0.11	20.09	9.26	16.18	
4275117	1146.8945	5.1	2.013042	0.12	1.29224	0.0139	1.0	0.62 ± 0.18	43.66 ± 3.33	34.05	11.09	3.64	T12
4552729	1427.64700	0.16	97.461490	0.62	4.174580	0.039153	1.1	0.47 ± 0.14	7.474 ± 0.078	44.69	10.07	3.68	PH
4858610	1128.2926	1.0	2.722874	0.18	1.17141	0.01202	0.61	0.57 ± 0.18	16.72 ± 0.30	32.15	12.00	5.18	
4927315	1077.3419	1.5	11.76856	1.5	1.9340	0.0192	1.2	0.67 ± 0.18	24.2 ± 1.1	31.24	17.07	3.49	T12
4951249	1072.5112	1.4	4.523406	0.24	1.29861	0.01574	0.62	0.55 ± 0.18	18.02 ± 0.59	40.99	11.01	6.36	T12
5008501	1073.17351	0.38	0.9680371	0.023	1.00558	0.01290	0.63	0.65 ± 0.18	55.4 ± 1.3	34.65	17.00	1.83	PH, T12
5023843	1320.7241	1.2	-358	-	6.1223	0.0543	1.5	0.3 ± 1.0	11.00 ± 0.15	-	-	2.83	PH
5128673	1353.1823	5.2	87.9654	36	2.25057	0.02746	0.44	0.1435 ± 0.0049	3.368 ± 0.048	28.37	8.66	2.81	blends
...

a A complete version of this table can be accessed from the online version and downloaded from <https://sites.google.com/site/largepunkenelephant/>

b Stars already identified as KOIs. The candidates presented here are transit signals that have not previously been detected in these systems.

c Planet candidates also identified by O12.

d Planet candidates classified as potential transit candidates by T12. If noted as T12_e, the same signal is identified as a different set of parameters by T12.

e The signal is selected by a different period originally and then corrected by visual inspection. The SNR and DSP reported here correspond to the period we report here instead of the selected period.

f Planet candidates classified as potential transit candidates by PlanetHunters. If noted as PHt, the transit feature is identified by PlanetHunters but the they did not report a period for comparison. These information can be accessed through <http://www.planethunters.org>.

g Systems may be blended by nearby stars. There exists a visible companion(s) within 20 square arcseconds in a 2MASS image stamp centered on the target star.

ACKNOWLEDGMENTS

We thank the *Kepler* team for the high quality public data, as well as the PlanetHunter team for their helpful comments. We also thank the anonymous referee for the insightful comments that greatly improved this paper. This research was partly funded by NSF grant AST-1108686.

REFERENCES

Ahmed, N. T., Natarajan, T. K. R., & Rao, K. R. 19 74, IEEE Trans. Computers, 90

Bakos, G., Noyes, R. W., Kovács, G., et al. 2004, PASP, 116, 266

Bakos, G. Á., Torres, G., Pál, A., et al. 2010, ApJ, 710, 1724

Bakos, G. Á., Hartman, J. D., Torres, G., et al. 2011, Detection and Dynamics of Transiting Exoplanets, St. Michel l’Observatoire, France, Edited by F. Bouchy; R. Díaz; C. Moutou; EPJ Web of Conferences, Volume 11, id.01002, 11, 1002

Batalha, N. M., Rowe, J. F., Bryson, S. T., et al. 2012, arXiv:1202.5852

Borucki, W. J., Koch, D., Basri, G., et al. 2010, Science, 327, 977

Borucki, W. J., Koch, D. G., Basri, G., et al. 2011, ApJ, 728, 117

Borucki, W. J., Koch, D. G., Basri, G., et al. 2011, ApJ, 736, 19

J. L. Christiansen, T. Barclay, J. M. Jenkins, et al., 2012, Kepler Data Release 14 Notes (KSCI-19054-001).

J. L. Christiansen, J. E. Van Cleve, J. M. Jenkins, et al., 2012, Kepler Data Characteristics Handbook (KSCI-19040-003).

Fischer, D. A., Schwamb, M. E., Schawinski, K., et al. 2012, MNRAS, 419, 2900

Ford, E. B., Ragozzine, D., Rowe, J. F., et al. 2012, arXiv:1201.1892

Gilliland, R. L., Jenkins, J. M., Borucki, W. J., et al. 2010, ApJ, 713, L160

Holman, M. J., Winn, J. N., Latham, D. W., et al. 2006, ApJ, 652, 1715

Jenkins, J. M., Caldwell, D. A., Chandrasekaran, H., et al. 2010, ApJ, 713, L87

Jenkins, J. M., Caldwell, D. A., Chandrasekaran, H., et al. 2010, ApJ, 713, L120

Jenkins, J. M., Chandrasekaran, H., McCauliff, S. D., et al. 2010, Proc. SPIE, 7740,

Kipping, D. M. 2008, MNRAS, 389, 1383

Kipping, D., & Bakos, G. 2011, ApJ 733, 36

Kipping, D. M., & Spiegel, D. S. 2011, MNRAS, 417, L88

Kovács, G., Zucker, S., & Mazeh, T. 2002, A&A, 391, 369

Kovács, G., Bakos, G., & Noyes, R. W. 2005, MNRAS, 356, 557

Koch, D. G., Borucki, W. J., Basri, G., et al. 2010, ApJ, 713, L79

Lintott, C. J., Schawinski, K., Slosar, A., et al. 2008, MNRAS, 389, 1179

Lintott, C., Schwamb, M. E., Sharzer, C., et al. 2012, arXiv:1202.6007

Loeb, A., & Gaudi, B. S. 2003, ApJ, 588, L117

P. Machalek, J. L. Christiansen, J. E. Van Cleve, et al., 2011, Kepler Data Release 9 Notes (KSCI-19049-001).

P. Machalek, J. L. Christiansen, J. E. Van Cleve, et al., 2010, Kepler Data Release 8 Notes (KSCI-19048-001).

Mandel, K., & Agol, E. 2002, ApJ, 580, L171

Mazeh, T., & Faigler, S. 2010, A&A, 521, L59

Murphy, S. J. 2012, MNRAS, 2509

Ofir, A., & Dreizler, S. 2012, arXiv:1206.5347

Pál, A., Bakos, G. Á., Torres, G., et al. 2008, ApJ, 680, 1450

Prša, A., Batalha, N., Slawson, R. W., et al. 2011, AJ, 141, 83

Rein, H., Payne, M. J., Veras, D., & Ford, E. B. 2012, arXiv:1204.0974

Schwamb, M. E., Lintott, C. J., Fischer, D. A., et al. 2012, ApJ, 754, 129

Sing, D. K. 2010, A&A, 510, A21

Smith, J. C., Stumpe, M. C., Van Cleve, J. E., et al. 2012, arXiv:1203.1383

Steffen, J. H., Fabrycky, D. C., Ford, E. B., et al. 2012, MNRAS, 421, 2342

Tenenbaum, P., Christiansen, J. L., Jenkins, J. M., et al. 2012, APJS, 199, 24

Yee, J. C., & Gaudi, B. S. 2008, ApJ, 688, 616